

Article

Comparative Evaluation of the Performance of the PTD and CSF Algorithms on UAV LiDAR Data for Dynamic Canopy Height Modeling in Densely Planted Cotton

Weiguang Yang^{1,2,3,†}, Jinhao Wu^{1,2,3,†}, Weicheng Xu⁴, Hong Li^{2,3,5}, Xi Li^{2,3,5}, Yubin Lan^{1,2,3}, Yuanhong Li^{1,2,3} and Lei Zhang^{2,3,5,*} 

- ¹ College of Electronic Engineering (College of Artificial Intelligence), South China Agricultural University, Guangzhou 510642, China; yangweiguang@stu.scau.edu.cn (W.Y.); wujinhao@stu.scau.edu.cn (J.W.); ylan@scau.edu.cn (Y.L.); liyuanhong@scau.edu.cn (Y.L.)
- ² Guangdong Laboratory for Lingnan Modern Agriculture, Guangzhou 510642, China; hongli_@stu.scau.edu.cn (H.L.); xili_@stu.scau.edu.cn (X.L.)
- ³ National Center for International Collaboration Research on Precision Agricultural Aviation Pesticide Spraying Technology, Guangzhou 510642, China
- ⁴ Guangdong Key Laboratory of New Technology for Rice Breeding, Rice Research Institute of Guangdong Academy of Agricultural Science, Guangzhou 510640, China; xuweicheng@gdaas.cn
- ⁵ College of Agriculture, South China Agricultural University, Guangzhou 510642, China
- * Correspondence: zhanglei@scau.edu.cn
- † These authors contributed equally to this work.

Abstract: This study introduces a novel methodology for the dynamic extraction of information on cotton growth in terms of height utilizing the DJI Zenmuse L1 LiDAR sensor mounted onto a DJI Matrice 300 RTK Unmanned Aerial Vehicle (UAV), aimed at enhancing the precision and efficiency of growth monitoring within the realm of precision agriculture. Employing the Progressive TIN Densification (PTD) and Cloth Simulation Filter (CSF) algorithms, combined with Kriging interpolation, we generated Canopy Height Models (CHMs) to extract the cotton heights at two key agricultural sites: Zengcheng and Tumxuk. Our analysis reveals that the PTD algorithm significantly outperforms the CSF method in terms of accuracy, with its R^2 values indicating a superior model fit for height extraction across different growth stages (Zengcheng: 0.71, Tumxuk: 0.82). Through meticulous data processing and cluster analysis, this study not only identifies the most effective algorithm for accurate height extraction but also provides detailed insights into the dynamic growth patterns of cotton varieties across different geographical regions. The findings highlight the critical role of UAV remote sensing in enabling large-scale, high-precision monitoring of crop growth, which is essential for the optimization of agricultural practices such as precision fertilization and irrigation. Furthermore, the study demonstrates the potential of UAV technology to select superior cotton varieties by analyzing their growth dynamics, offering valuable guidance for cotton breeding and cultivation.

Keywords: LiDAR; dynamic height growth; densely planted cotton



Citation: Yang, W.; Wu, J.; Xu, W.; Li, H.; Li, X.; Lan, Y.; Li, Y.; Zhang, L. Comparative Evaluation of the Performance of the PTD and CSF Algorithms on UAV LiDAR Data for Dynamic Canopy Height Modeling in Densely Planted Cotton. *Agronomy* **2024**, *14*, 856. <https://doi.org/10.3390/agronomy14040856>

Academic Editor: Maofang Gao

Received: 18 March 2024

Revised: 11 April 2024

Accepted: 16 April 2024

Published: 19 April 2024



Copyright: © 2024 by the authors. Licensee MDPI, Basel, Switzerland. This article is an open access article distributed under the terms and conditions of the Creative Commons Attribution (CC BY) license (<https://creativecommons.org/licenses/by/4.0/>).

1. Introduction

Among various crops, cotton holds a pivotal role due to its extensive use in the textile industry and its significant economic value, particularly in developing countries [1]. Cotton farming has undergone substantial technological transformations, including the adoption of genetically modified seeds, advanced pest management techniques, and high-efficiency irrigation systems [2–5]. These innovations not only enhance yield and quality but also address environmental concerns by reducing the use of water, fertilizers, and pesticides.

The core of precision agriculture lies in the ability to monitor and manage crop growth with unprecedented accuracy. In this regard, the emergence of Unmanned Aerial Vehicles (UAVs) equipped with LiDAR (Light Detection and Ranging) technology has opened up new

horizons [6–9]. Unlike the traditional methods, UAV-borne LiDAR provides high-resolution, three-dimensional information about the crop canopy, enabling precise measurements of plants' height, density, and biomass [10–12]. Furthermore, LiDAR technology captures the detailed 3D structures of the terrain and canopy, offering unparalleled accuracy and efficiency in crop growth analysis. Large-scale research has been undertaken in the agricultural field [13–15]. For densely planted cotton, where manual measurements are impractical, UAV-borne LiDAR offers a promising solution for monitoring canopy height and detecting growth variations [9,16], which are crucial for optimizing irrigation, fertilization, and pest management strategies.

The measurement of canopy height plays a pivotal role in the management of cotton crops [17–19]. It serves as a critical indicator of plant health, vigor, and development stage, directly influencing decisions related to irrigation, nutrient management, and pest control. In densely planted cotton fields, uniform canopy development is crucial for optimizing light interception and photosynthesis, thereby enhancing the yield potential [20–22]. Furthermore, accurate and timely data on canopy height can aid in identifying growth discrepancies within fields, enabling targeted interventions to address issues such as nutrient deficiencies or water stress before they impact overall production [23,24].

Implementing UAV-borne LiDAR technology in densely planted cotton fields presents both challenges and opportunities [16]. One of the main challenges is navigating the complex canopy structure of dense cotton crops, where overlapping leaves and branches can obscure the view of the plant bases, complicating accurate height measurements [25,26]. Additionally, the variability in cotton plant morphology across different varieties and growth stages requires sophisticated algorithms capable of accurately interpreting LiDAR data [27,28].

Despite these challenges, the integration of UAV-borne LiDAR technology into cotton farming offers significant opportunities. By providing high-resolution, three-dimensional insights into the canopy structure, LiDAR technology enables more precise management of crop health and productivity [29–31]. It facilitates the identification of areas within a field experiencing growth issues, allowing for more targeted and efficient use of resources. Moreover, the ability to rapidly collect and analyze data over large areas makes UAV-borne LiDAR an invaluable tool for large-scale cotton farming operations, promoting sustainable agricultural practices and improving yield quality and quantity.

The culmination of this study is aimed at harnessing the synergistic potential of UAV-borne LiDAR technology, sophisticated algorithms, and geospatial analysis to revolutionize the precision farming landscape, particularly in the context of cotton agriculture. The research objectives outlined provide a clear pathway towards achieving unprecedented accuracy in canopy height estimation, enabling the selection of superior cotton varieties across diverse geographical regions and within the same locality.

Through comprehensive data collection in the cotton fields of Zengcheng and Tumxuk using UAV-borne LiDAR, this study endeavors to integrate the CSF algorithm [32,33] and the PTD algorithm [8,34] with Kriging interpolation to construct Canopy Height Models (CHMs). This novel approach not only facilitates the extraction of cotton canopy height information with remarkable precision but also allows for comparative analysis against manually measured canopy heights, thereby validating the efficacy of the methodologies employed. By harnessing the power of these emerging technologies, farmers and agricultural scientists can gain a deeper understanding of crop dynamics, leading to more informed decision-making and ultimately more sustainable and productive farming practices.

2. Materials and Methods

Aligned with the objectives of leveraging UAV-borne LiDAR technology for accurate canopy height information extraction in densely planted cotton fields, this section delineates the comprehensive field experiment design. The study encapsulates the fusion of high-resolution aerial data acquisition with advanced processing algorithms to navigate the challenges of precision agriculture in cotton farming. The experiments, conducted

across distinct climatic zones in Tumxuk, Xinjiang, and Zengcheng, Guangdong (Figure 1), provide a broad spectrum of data pertinent to the canopy height dynamics under varied environmental conditions.

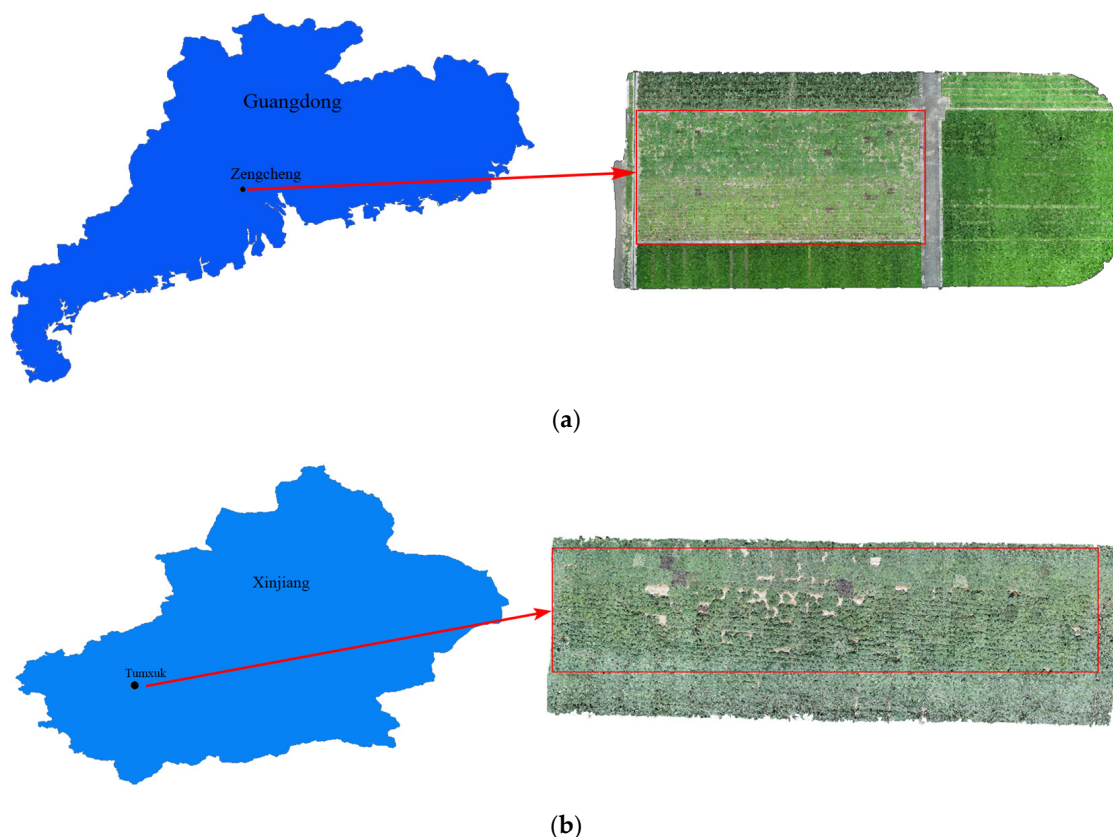


Figure 1. Overview of the experimental area. (a) Zengcheng (the area of the test area is 2000 m², marked with a red box); (b) Tumxuk (the area of the test area is 1600 m², marked with a red box).

2.1. Experimental Site Description

Tumxuk, located on the eastern edge of the Taklamakan Desert, features flat terrains predominantly characterized by desert and saline–alkali soils. This region experiences a temperate continental arid climate, with hot, dry summers and cold winters. Precipitation is scant, averaging around 100 mm annually, primarily concentrated in the summer months. Tumxuk boasts an average annual sunshine duration of approximately 2500 h. The field experiment in Tumxuk was carried out at the 44th Regiment of the Third Division’s National Precision Agriculture Aviation Pesticide Application Technology International Joint Research Center (E 78°39′51″, N 39°50′17″).

Zengcheng, situated within the Pearl River Delta economic zone, offers relatively flat and fertile lands. It is under the influence of a subtropical monsoon climate, marked by hot, humid summers and mild, dry winters. The area receives ample rainfall, with an annual average of about 1700 mm, predominantly during the summer. The region enjoys 1800–2000 h of sunlight annually. The Zengcheng experiment was conducted at the National Precision Agriculture Aviation Pesticide Application Technology International Joint Research Center (E 113°35′40″, N 23°20′39″).

2.2. Experiment Design

The trial in Tumxuk encompassed 306 cotton varieties, with each variety represented by a plot, totaling 306 plots. The sowing pattern was one film with three rows, with a row spacing of 76 cm and a plant spacing of 25 cm. The inter-plot spacing was maintained at

75 cm, with a sowing depth of 2–3 cm, placing one seed per hole, and each plot consisting of 21 holes. Sowing occurred on 15 April 2023, with germination observed by 18 April 2023.

Similarly, the trial in Zengcheng featured 306 cotton varieties across 306 plots. The cultivation method involved ridge planting, with a ridge distance of 40 cm and a ridge width of 110 cm. Each ridge hosted two rows of cotton, with row spacing of 70 cm and plant spacing of 25 cm. The plots were separated by a 75 cm gap, the sowing depth was set at 2–3 cm, with two seeds per hole, and each plot comprised 10 holes. Sowing took place on 7 March 2023, with seedlings emerging by 10 March 2023.

2.3. Data Collection and Preprocessing

2.3.1. Data Collection

In alignment with the study's objective to harness UAV-borne LiDAR for accurate canopy height estimation in densely planted cotton fields, a comprehensive data collection methodology was devised. This methodology emphasizes the synergy between advanced remote sensing technology and meticulous ground truth measurements, aiming to optimize the precision and reliability of canopy height data across the critical growth phases for cotton.

The data acquisition was conducted under optimal weather conditions, specifically on clear days between 9:00 a.m. and 8:00 p.m., to ensure maximum visibility and data accuracy. The DJI Matrice 300 RTK (DJI, Shenzhen, China) UAV, equipped with the extensively tested Zenmuse L1 LiDAR sensor (DJI, Shenzhen, China) [35–37], was selected for its advanced capabilities, including its superior anti-magnetic interference, precise positioning, and intelligent flight modes, such as obstacle avoidance and auto-return. These features significantly enhance the safety and efficiency of flight operations. The Zenmuse L1 sensor, integrating a Livox LiDAR module, high-precision IMU, a mapping camera, and a three-axis gimbal, guarantees an effective point cloud density of 99.99%, even in motion, ensuring comprehensive coverage and detail of the cotton canopy (Figure 2a).

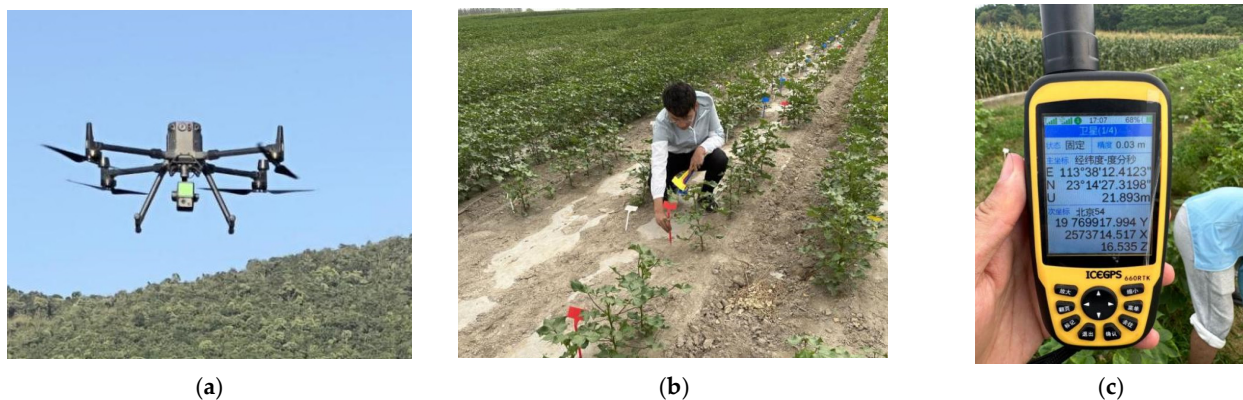


Figure 2. Data collection overview. (a) DJI Matrice 300 RTK UAV and Zenmuse L1 LiDAR; (b) Ground truth sample marking; (c) Ice Glacier GPS receiver.

Scheduled bi-weekly from the flowering to the boll-opening stages, the UAV missions were carefully planned to capture the dynamic growth patterns of the cotton. The flights were conducted at a 20 m altitude, with a 1 m/s speed, ensuring an 80.0% overlap rate in both the flight and lateral directions and a 10% LiDAR lateral overlap rate. The double echo mode was activated to enhance the point cloud quality, achieving a density of 7071 points/m². Each mission, lasting about 10 min, was executed between 9:00 a.m. and 8:00 p.m., when the conditions were ideal for data capture. Subsequently, the collected point cloud data were stitched together and saved in LAS format for analysis.

The ground truth measurements were conducted in parallel with the UAV data collection. In each of the 306 plots in both Tumxuk and Zengcheng, three cotton plants were randomly selected, marked with color-coded tags for consistent identification across all the

data collection sessions. The plants' height was measured from the ground to the 3rd or 4th leaf from the top of the canopy using a tape measure, with the precision recorded to the nearest centimeter (Figure 2b).

The Ice Glacier GPS receiver, with the Qianxun Spatial Intelligence Inc. (Shanghai, China) network differential positioning service for real-time kinematics (RTK) surveying, was used to determine the actual coordinates of the ground sampling points (Figure 2c). This system uses satellite navigation and ground station data to achieve a centimeter-level positioning accuracy, significantly surpassing traditional GPS technology. With an error margin within 2 cm, the Ice Glacier RTK system was instrumental in precisely demarcating the experimental areas and ensuring the accuracy and repeatability of the data collection. By positioning the GPS directly above the target plant, the exact geographical coordinates of each cotton plant were obtained, further validating the remote sensing data collected via the UAV.

2.3.2. Data Preprocessing

The data preprocessing was conducted on a system running Windows 10, powered by an AMD Ryzen 7 5700X 8-Core processor and 128 GB of RAM, with an NVIDIA GeForce RTX 3060 graphics card featuring 12 GB of video memory. This robust computing setup facilitated the handling of large point cloud datasets, enabling efficient data manipulation and analysis.

The M300 UAV, equipped with the Zenmuse L1 LiDAR sensor, generated point cloud data files during the flight missions. These files, including formats such as CLC, CLI, and CMI, encapsulated 3D information on the surveyed cotton fields. Using DJI Terra software (DJI, V3.9.2), these files were stitched together and converted into the LAS format for further processing.

Given the substantial size of each dataset, typically around 2 GB, it was imperative to enhance the processing efficiency. The LiDAR360 software (GreenValley International, Berkeley, CA, USA, V5.2.2) was utilized to crop the datasets, retaining only the relevant point cloud data on the experimental fields. This step reduced the file sizes to approximately 1 GB, significantly speeding up the preprocessing workflow. Figure 3a illustrates the outcome of the cropping process, showcasing the delineated experimental fields.

The removal of noise from the point cloud data was paramount to preserving the integrity of the information pertinent to the cotton crops. Manual denoising was employed using the LiDAR360 software, which, despite being time-consuming, ensured the preservation of crucial data characteristics. This method was preferred over automated algorithms to prevent the unnecessary loss of ground points, which are critical for accurate plant height extraction. Figure 3b depicts the denoising results, with panel (a) displaying the original data with apparent noise and panel (b) showing the cleaned data post-manual denoising.

2.4. Cotton Plant Height Extraction Algorithms

2.4.1. The Cloth Simulation Filter (CSF) Algorithm

The CSF algorithm is a novel approach used to simulate a cloth or fabric model in computer programs, representing ground surfaces in this context. In this model, particles connected by virtual springs subject to Hooke's Law mimic the flexibility and dynamics of fabric, as shown in Figure 4. These particles, while dimensionless, possess mass and are interconnected, forming a network that simulates cloth's behavior over a 3D landscape. The primary function of these connections is to establish the positioning of the particles within the cloth, thereby simulating the ground's shape based on the constraints imposed by neighboring particles.

The overall workflow of the CSF algorithm, illustrated in Figure 5, involves inverting the original point cloud, overlaying the cloth model, and analyzing the positional constraints of the cloth nodes to mimic and determine the ground's shape. This process effectively distinguishes ground points from non-ground points (such as buildings or

vegetation) by simulating the cloth's descent under gravity, halting at ground points and sagging at non-ground points.

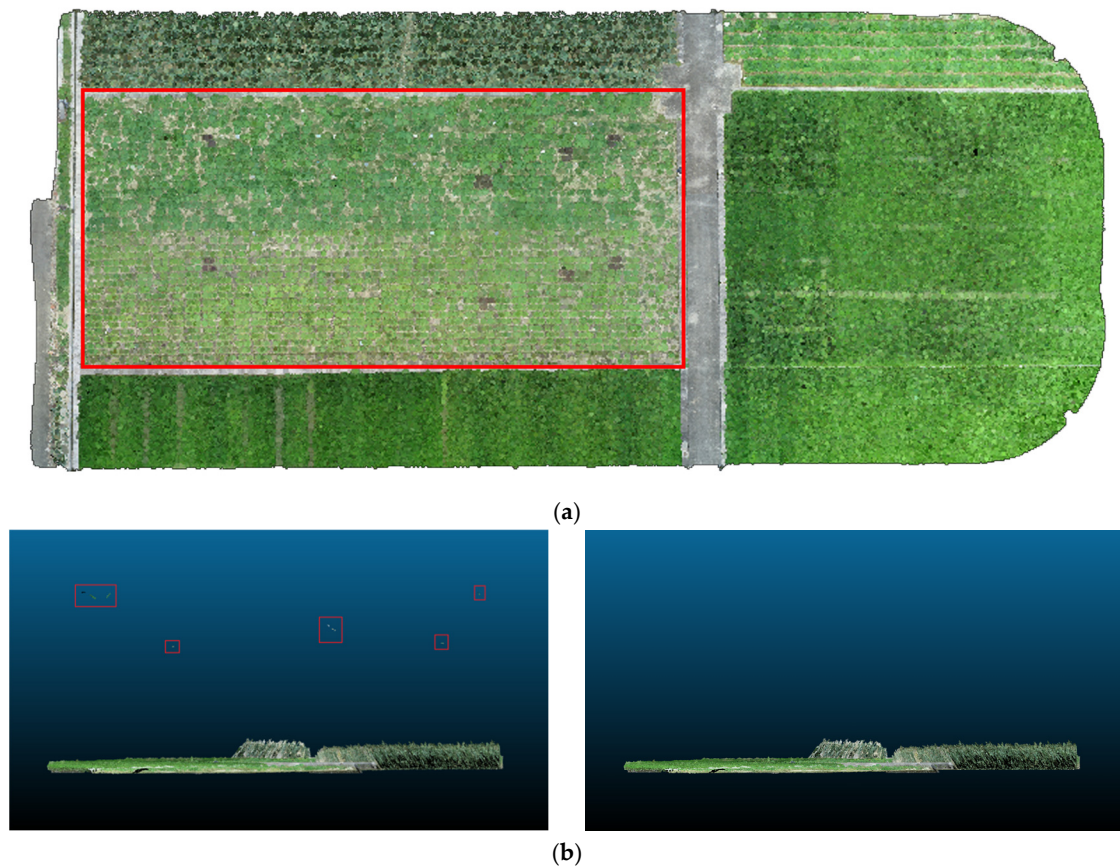


Figure 3. Data preprocessing. (a) Experimental field (the red box is the test area); (b) denoising point cloud data (the red box is noise).

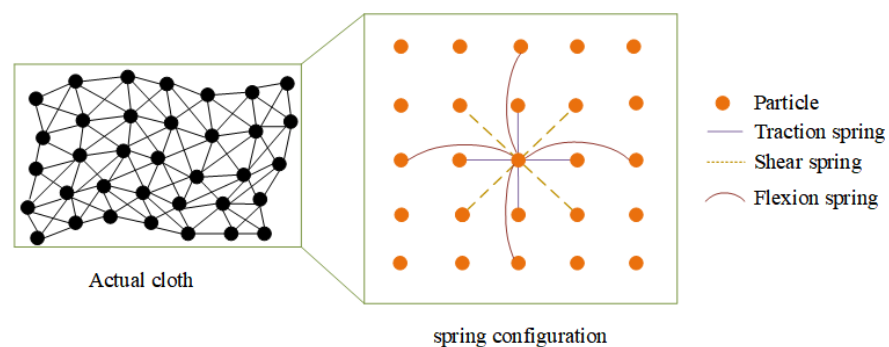


Figure 4. Cloth model. (Reference from Forests 2023 [38]; Figure 2).

The application of the CSF algorithm in cotton plant height information extraction hinges on its capability to accurately identify ground points. By constructing a precise ground model, the height difference between the cotton plant point clouds and the ground model derived from LiDAR data enables the calculation of the plant heights. The efficiency and automation level of the CSF algorithm make it adept at processing large datasets and adaptable to complex terrains.

In this research, the CSF algorithm parameters were configured as follows: cloth grid resolution was set to 0.7 pixels per inch; cloth stiffness parameter was fixed at 2; maximum iterations were capped at 500; and the distance threshold between the point cloud data and the cloth simulation points was established at 0.5 m.

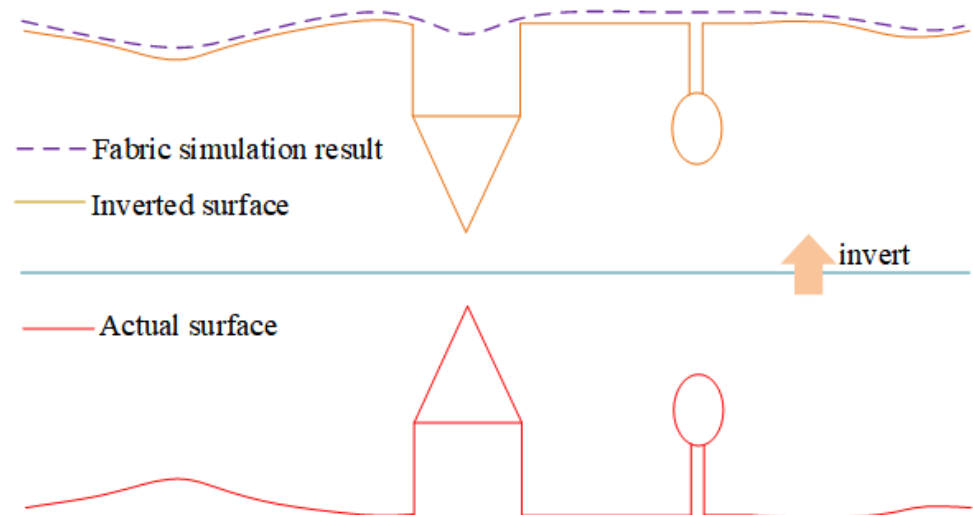


Figure 5. CSF algorithm. (Reference from Forests 2023 [38]; Figure 1).

2.4.2. The Progressive TIN Densification (PTD) Algorithm

The PTD algorithm, another widely utilized method for ground point extraction in remote sensing, employs a progressive strategy to build and refine a Triangular Irregular Network (TIN) for identifying ground points. This approach incrementally integrates the points from the point cloud into the TIN, updating it until all the ground points are recognized.

The initialization of the PTD algorithm involves selecting seed points from the point cloud to construct the initial TIN (Figure 6). Subsequently, the remaining points are evaluated for inclusion based on their vertical distance to the nearest TIN surface and their projection within the TIN. Points are added to the TIN if their vertical distance is below a predefined threshold and their projection lies within a TIN surface, thereby refining the TIN structure.

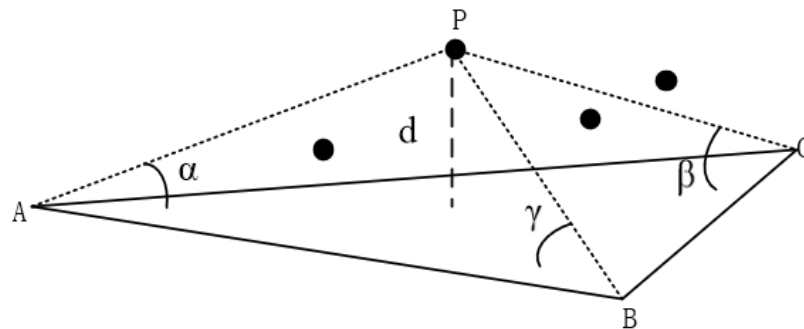


Figure 6. Calculated values of data points during TIN encryption.

The PTD algorithm's adaptability to varying terrain undulations makes it especially useful for accurate ground modeling and plant height measurement in areas with significant topographical changes. However, setting the appropriate thresholds is crucial and requires adjustment based on the specific scenarios and data characteristics.

In this research, the PTD algorithm parameters were configured as follows: scene type was set to gentle slopes; maximum building size was established at 20 m; maximum terrain slope was configured to 60 degrees; iteration angle was set at 8 degrees; iteration distance was determined to be 1.4 m; and triangulation construction was halted when the addition of vertices dropped below 10.

2.4.3. The Kriging Interpolation Method

Kriging is a statistical interpolation method that estimates the numerical values at unsampled locations based on the spatial autocorrelation among the sample points. It assumes that points closer to each other are more similar, thereby calculating the weights for the sample points based on their distance and spatial correlation with the interpolation point.

The essence of Kriging lies in its ability to model spatial trends (trend term) and random fluctuations (residual term) in data, allowing for the estimation of the values at unsampled locations using a formula that incorporates the weighted sum of the observed values.

Kriging's effectiveness in spatial data interpolation, coupled with its application to accurately estimating cotton plant heights, showcases its utility in precision agriculture. By modeling the spatial variability within cotton fields, Kriging aids in refining the elevation data obtained using the CSF and PTD algorithms, further enhancing the accuracy of the plant height measurements.

Kriging interpolation employs a 0.3 grid size for delineating spatial extents. The Gaussian variogram model refines the spatial correlations. Reshaping and filtering the grid, only pertinent elevation points are included before executing the interpolation to approximate a continuous spatial surface.

2.5. Accuracy Assessment

The following section details the approach employed to assess the precision of the cotton plant height information extraction techniques utilized in this study, leveraging established statistical metrics.

RMSE is a widely used metric to quantify the deviation between predicted values and observed measurements. It offers a standard means of assessing the accuracy of a predictive model. The formula for RMSE is given as follows:

$$\text{RMSE} = \sqrt{\frac{1}{n} \sum (\hat{y}_i - y_i)^2}$$

A lower RMSE value indicates a higher-precision predictive model, suggesting that the extracted cotton plant heights closely align with the ground truth measurements.

MAE measures the average magnitude of the errors between the predicted values and the actual observations, without considering their direction. It is defined as:

$$\text{MAE} = \frac{1}{n} \sum |y_i - \hat{y}_i|$$

A lower MAE value reflects a model's higher level of accuracy, indicating that the discrepancies between the predicted and observed plant heights are minimal.

The R^2 metric gauges the degree of correlation between the model's predicted values and the actual observations. It illustrates how well the predicted values from the model fit the observed data. An R^2 value closer to 1 signifies that the model predictions closely match the observed values, showcasing a high degree of accuracy in the model's predictions.

$$R^2 = 1 - \frac{\sum (y_i - \hat{y})^2}{\sum (y_i - \bar{y})^2}$$

In the above formula, where y_i represents the observed plant heights, \hat{y}_i denotes the predicted plant heights from the model, and n is the number of samples.

2.6. Data Analysis

To elucidate the dynamic growth patterns and categorize the variability within densely planted cotton fields, an integrated approach employing the Elbow Method and K-means clustering was adopted. This dual-faceted analysis framework is pivotal to understanding the intricate growth dynamics and optimizing the precision in cotton cultivation

management, aligning with the overarching goal of enhancing yield through advanced agricultural practices.

2.6.1. The Elbow Method for Optimal Cluster Determination

For a range of K-values, typically from 1 to 10, the K-means clustering algorithm is applied, and the sum of squared errors (SSE) for each K is computed. The SSE represents the sum of the squared distances between each data point and its nearest cluster center, capturing the compactness of the clusters.

The SSE values are plotted against their corresponding K-values, creating a curve that illustrates how the SSE varies with different numbers of clusters. This curve serves as the basis for identifying the optimal number of clusters.

The “elbow point” on the SSE curve is identified as the point where the rate of the decrease in the SSE sharply transitions from rapid to gradual. This inflection signifies that additional clusters beyond this point only marginally improve the model’s fit, thus providing a heuristic measure for selecting the optimal K-value [39].

2.6.2. K-Means Clustering

Step 1: Selection of Cluster Number (K). The number of clusters, K, is a crucial parameter that is determined based on domain knowledge, the Elbow Method, and other statistical measures, such as the silhouette score.

Step 2: Cluster Center Initialization. Initial cluster centers are randomly selected from the data points, or using methods like K-means++ to enhance the selection process, ensuring a diverse starting point for the clustering.

Step 3: Assignment of Data Points. Each data point in the dataset is assigned to the nearest cluster center based on Euclidean distance, grouping similar height data points together.

Step 4: Updating Cluster Centers. For each cluster, the mean position of all the assigned points is calculated, and this mean becomes the new cluster center, refining the cluster composition.

Step 5: Iteration Until Convergence. Steps 3 and 4 are repeated until the cluster centers stabilize and no further changes are observed, indicating that the algorithm has converged.

The simplicity and intuitive nature of K-means clustering, coupled with the heuristic insight provided by the Elbow Method, make this analytical framework particularly suited for parsing the complex data derived from UAV-borne LiDAR scans of cotton fields. By efficiently segregating the plant height data into distinct clusters, this methodology aids in discerning patterns and anomalies in the growth trends across different cotton varieties and developmental stages. The integration of these techniques fosters a deeper understanding of plant height variability, which is instrumental in crafting targeted agricultural interventions to boost cotton yield and quality, thereby advancing the goals set forth in the study’s introduction.

3. Results

3.1. Cotton Plant Height Extraction

In pursuit of the study’s objective to accurately estimate cotton canopy heights using UAV-borne LiDAR, this section delves into the results garnered from the implementation of the Cloth Simulation Filter (CSF) and Progressive TIN Densification (PTD) algorithms. The approach to cotton plant height information extraction was methodically structured, starting from data acquisition to the derivation of the Canopy Height Model (CHM) and eventual estimation of the plant heights.

Utilizing the DJI Matrice 300 RTK (M300) UAV equipped with the L1 LiDAR sensor, the point cloud data for the experimental fields were collected. These data underwent preprocessing steps such as stitching and denoising, followed by ground and non-ground separation using the CSF algorithm implemented via Python (V3.9, dependent library laspy, etc.). The CSF algorithm’s parameters were meticulously calibrated to optimize the

segmentation process. Subsequently, Kriging interpolation was employed to generate a Digital Surface Model (DSM) and Digital Elevation Model (DEM), which were combined to produce the CHM using band math operations. Figure 7 illustrates a flowchart of the CSF algorithm-based height extraction process. Taking the flowering phase data from the Tumxuk experimental field as the case study, the CSF algorithm segmented the point cloud data into ground and non-ground points with specific parameters set for the cloth grid resolution, stiffness, iteration count, and distance threshold. The generated DSM and DEM were processed in LiDAR360 software to obtain the CHM, depicted in Figure 7.

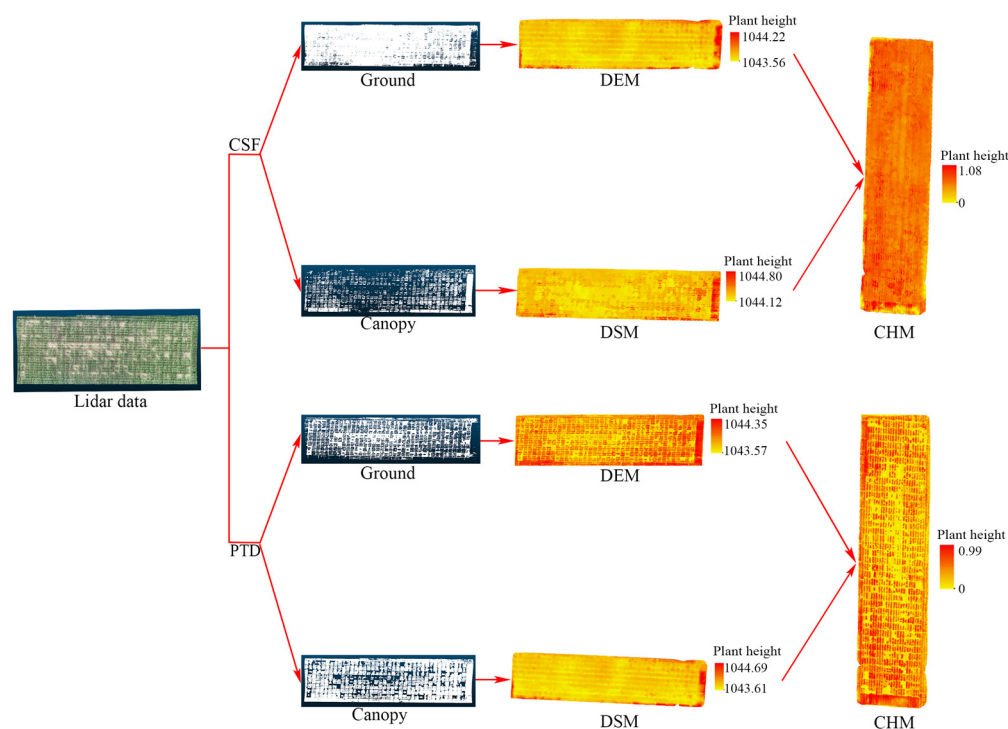


Figure 7. Comprehensive workflow for CHM generation from UAV LiDAR data. This diagram illustrates the sequential steps in processing LiDAR data to construct Canopy Height Models (CHMs), starting with the application of Cloth Simulation Filter (CSF) and Progressive TIN Densification (PTD) algorithms for ground and canopy point discrimination. The workflow includes the creation of a Digital Elevation Model (DEM) and a Digital Surface Model (DSM), leading to the final CHM by contrasting the DSM and DEM layers.

Similar to the CSF approach, the PTD algorithm was applied to point cloud data pre-processed for noise and irrelevant data removal. The PTD algorithm, known for its efficacy in complex terrains, was configured with specific settings suitable for the experimental field's characteristics. The generated DSM and DEM from Kriging interpolation were analyzed to derive the CHM. The workflow of the PTD algorithm-based method is visualized in Figure 7. The PTD algorithm's parameterization was tailored to the landscape features of the Tumxuk field, focusing on the slope settings, maximum building size, terrain gradient, and iteration specifics. The DSM and DEM obtained using this algorithm facilitated the creation of the CHM, as shown in Figure 7.

The final step involved integrating the derived CHMs with the actual geographic coordinate data within ArcMap software (Esri, Redlands, CA, USA, V10.8). The precision of the handheld Ice Glacier RTK, with a 2 cm accuracy, necessitated the establishment of a buffer zone for accurate height matching. Through statistical analysis within these buffer zones, the maximum height value was selected as the estimated plant height for each coordinate. To enhance visibility and accuracy, the buffer zones were set to a diameter of 30 cm for illustrative purposes, as demonstrated in Figure 8.



Figure 8. Plant height (CHM) extraction sampling points and buffer zone. Panel (a) shows the distribution of sampling points across the cotton field, where plant heights are extracted from CHM data. Panel (b) illustrates the established 30 cm buffer zones around each sampling point, used to accurately match canopy height values from geographic coordinate data within the ArcMap software.

3.2. Accuracy Assessment of Cotton Plant Height Information Extraction

The CSF algorithm was applied to two sets of point cloud data from Zengcheng and three sets from Tumxuk, extracting the estimated plant heights for comparison with the ground truth measurements. The fitting results, displayed in Figure 9a (Zengcheng) and Figure 9b (Tumxuk), demonstrate the algorithm's performance across different growth stages, including the flowering, boll-forming, and boll-opening periods.

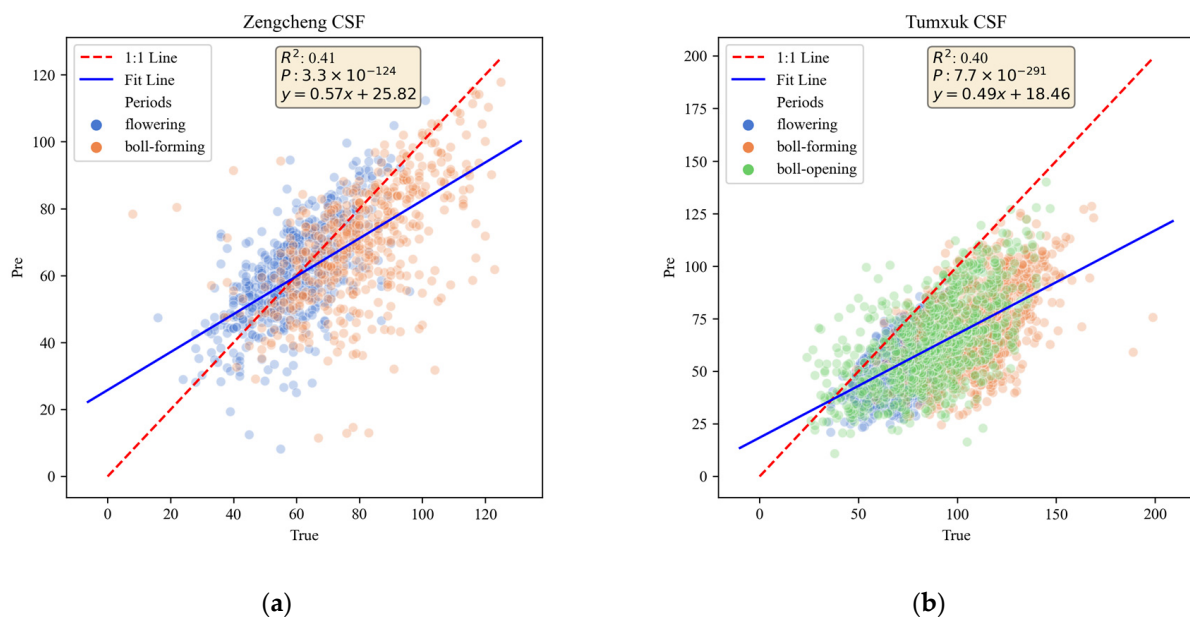


Figure 9. Plant height calculated using CSF algorithm and actual measured value. (a) Zengcheng; (b) Tumxuk.

Similarly, the PTD algorithm was tested on the same datasets from Zengcheng and Tumxuk, with the objective of comparing the algorithm-derived height estimates against the ground-measured data. The fitting outcomes, as shown in Figure 10a (Zengcheng) and Figure 10b (Tumxuk), reveal the algorithm's efficacy in height estimation across various growth stages.

The accuracy of the cotton plant heights extracted using the CSF and PTD algorithms was assessed using a set of statistical measures (Table 1): the coefficient of determination (R^2), Root Mean Squared Error (RMSE), and Mean Absolute Error (MAE). These metrics provided insight into the precision and reliability of the plant height estimates derived from the UAV-borne LiDAR data in the distinct agricultural settings of Zengcheng and Tumxuk.

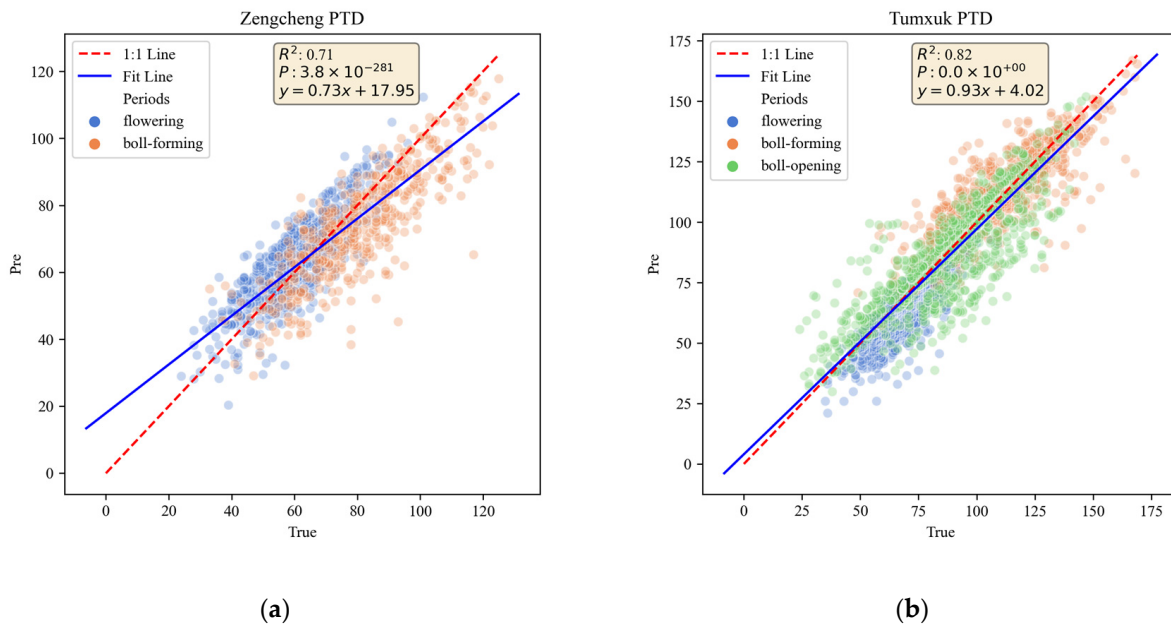


Figure 10. Plant height calculated using PTD algorithm and actual measured value. (a) Zengcheng; (b) Tumxuk.

Table 1. Accuracy evaluation of the two algorithms in each period.

Method	Location	Periods	R ²	RMSE (cm)	MAE (cm)
CSF	Zengcheng	flowering	0.4434	11.6684	9.1448
		boll-forming	0.3380	19.4277	14.1307
		all	0.4078	15.7813	11.4777
	Tumxuk	flowering	0.2245	21.2403	17.1366
		boll-forming	0.2799	43.0986	39.3086
		boll-opening	0.3697	31.2330	26.2427
all	0.4019	33.3241	27.5602		
PTD	Zengcheng	flowering	0.7112	8.8591	7.2769
		boll-forming	0.7019	10.6853	8.8164
		all	0.7064	10.1510	7.9983
	Tumxuk	flowering	0.7429	8.5152	6.4152
		boll-forming	0.6749	10.0503	7.7189
		boll-opening	0.6858	12.4963	10.2013
all	0.8249	10.7192	8.1128		

In Zengcheng, the CSF algorithm resulted in a lower R² of 0.4078, indicating a moderate correlation between the estimated and actual plant heights. The RMSE and MAE values, standing at 15.7813 cm and 11.4777 cm, respectively, further reflect the discrepancies in the height estimates. Conversely, the PTD algorithm demonstrated superior accuracy with an R² of 0.7064, suggesting a strong correlation between the estimated and ground truth heights. The RMSE and MAE were significantly lower at 10.1510 cm and 7.9983 cm, respectively, underscoring the PTD algorithm’s enhanced precision in plant height estimation in Zengcheng.

Similarly, in Tumxuk, the CSF algorithm produced an R² of 0.4019, an RMSE of 33.3241 cm, and an MAE of 27.5602 cm. These metrics indicate a comparable level of accuracy to that observed in Zengcheng, with considerable room for improvement in the height estimation accuracy. The performance of the PTD algorithm in Tumxuk was markedly better, yielding an R² of 0.8249, which suggests a very high degree of correlation between the estimated and actual plant heights. The RMSE and MAE were significantly reduced to 10.7192 cm

and 8.1128 cm, respectively, highlighting the PTD algorithm’s robustness and reliability in extracting plant heights in the challenging environment of Tumxuk.

3.3. Cotton Plant Height Growth Dynamics

In Zengcheng, the cotton plant heights were extracted using the PTD algorithm in conjunction with the ground truth coordinates. Starting from the emergence date of 10 March 2023, the growth dynamics were plotted with days after emergence on the x-axis and the cotton plant heights on the y-axis. Six sets of point cloud data were collected on various dates, illustrating the growth trend over the entire cycle, as shown in Figure 11a.

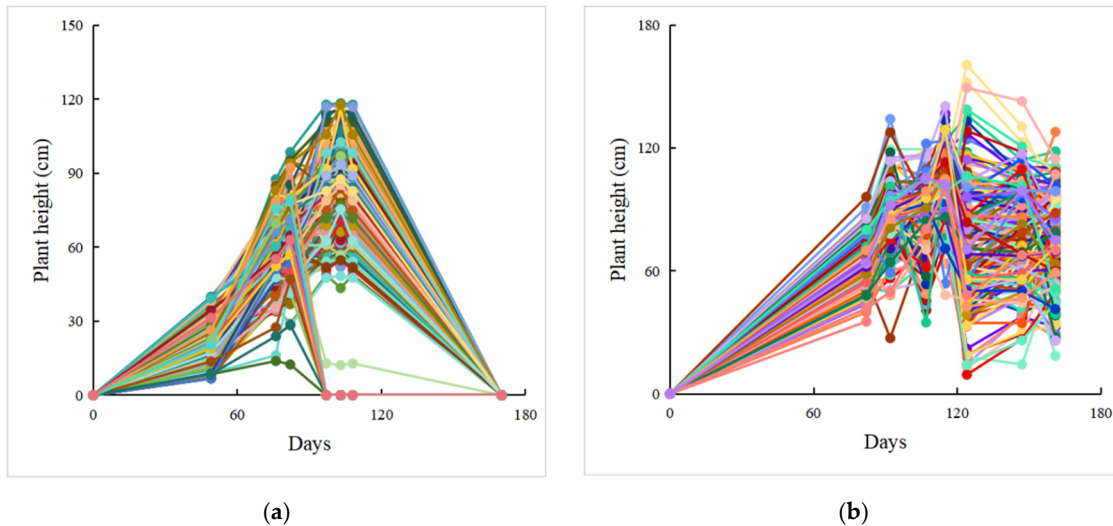


Figure 11. Dynamic growth curves of cotton varieties. Panel (a) illustrates the growth progression of 306 cotton varieties in the Zengcheng test area, plotted over the entire growth cycle with plant height against days after emergence, using the PTD algorithm for height extraction. Panel (b) depicts analogous growth trajectories for the Tumxuk test area.

Similarly, in Tumxuk, the plant heights were determined using the PTD algorithm. With an emergence date of 15 April 2023, seven point cloud datasets were collected, reflecting the dynamic growth of cotton over the cycle. The growth trend is visualized in Figure 11b, highlighting significant growth stages.

Given the dense nature of the growth dynamics curves in Figure 11, cluster analysis was performed to facilitate a clearer analysis. The Elbow Method estimated the optimal number of clusters, indicating a significant decrease in the sum of squared errors (SSE) up to 4 clusters, beyond which the reduction in the SSE becomes negligible. This suggests that four clusters represent a balanced trade-off between the number of clusters and cluster quality, as illustrated in Figure 12.

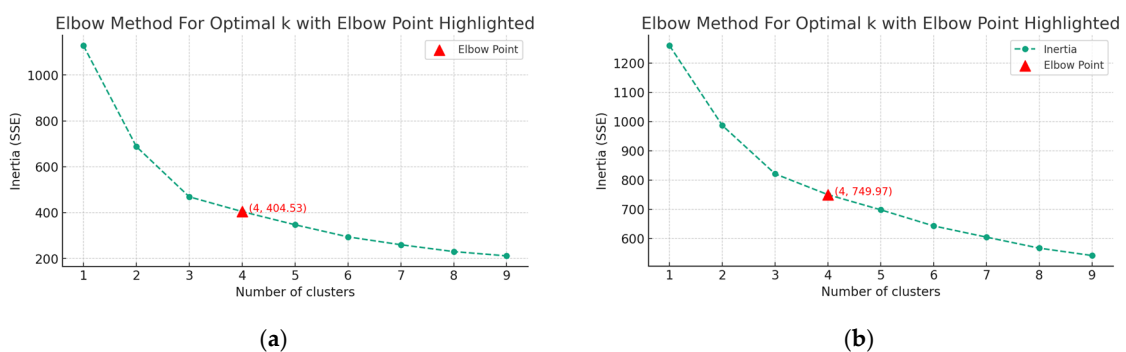


Figure 12. Cluster number calculation based on Elbow Method. (a) Zengcheng; (b) Tumxuk.

The clustered growth dynamics, shown in Figure 13, display variations in the growth rates among different cotton varieties over time, with each color representing a distinct cluster.

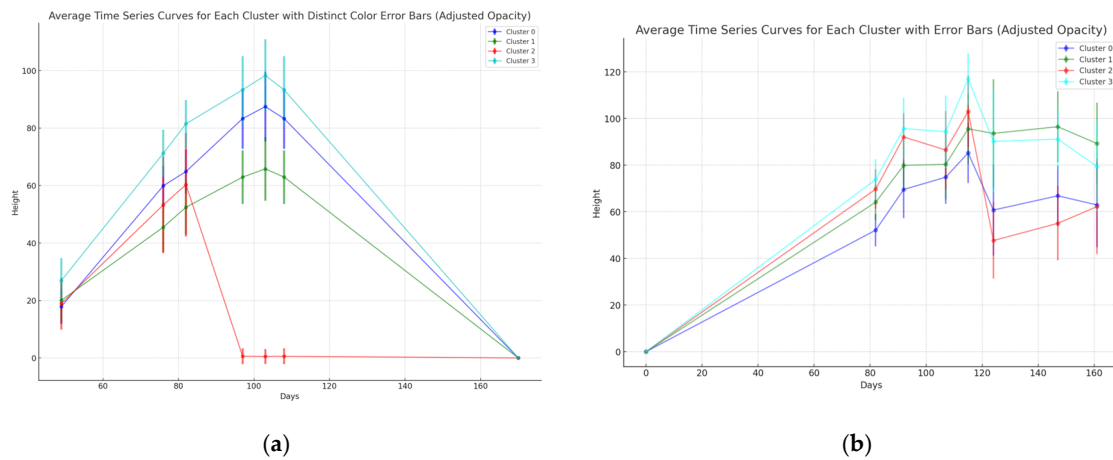


Figure 13. Average growth curve for each category. (a) Zengcheng; (b) Tumxuk.

Table 2 (Zengcheng) and Table 3 (Tumxuk) present the mean plant heights for different clusters at various growth stages. A comparative analysis between regions and among varieties revealed the following. Regional Comparison: In Zengcheng, the clusters showed varying growth rates, with Cluster 3 demonstrating rapid growth, especially between 49 and 76 days. Tumxuk displayed faster growth rates in all the clusters, particularly between 82 and 92 days, compared to Zengcheng. Varietal Comparison: In both Zengcheng and Tumxuk, specific clusters exhibited faster growth rates during certain periods, with Cluster 3 in Zengcheng and Cluster 1 in Tumxuk showing the most vigorous growth. The analysis suggests that Cluster 3 in Zengcheng and Cluster 1 in Tumxuk are more robust in their growth dynamics compared to the other clusters.

Table 2. Height mean value of Zengcheng cotton plant in each cluster.

Cluster Height (cm) Days	0	49	76	82	97	103	108	170
0	0.00	17.89	59.92	64.87	83.29	87.45	83.29	0.00
1	0.00	20.07	45.51	52.45	62.93	65.78	62.93	0.00
2	0.00	18.92	53.28	60.30	0.59	0.55	0.59	0.00
3	0.00	26.96	71.23	81.48	93.31	98.29	93.31	0.00

Table 3. Height mean value of Tumxuk cotton plant in each cluster.

Cluster Height (cm) Days	0	82	92	107	115	124	147	161
0	0.00	52.13	69.57	74.85	85.27	60.73	66.86	62.95
1	0.00	64.12	79.91	80.37	95.60	93.64	96.50	89.29
2	0.00	69.72	92.09	86.50	103.00	47.66	55.04	62.22
3	0.00	73.87	95.68	94.37	116.94	90.20	91.18	79.48

The growth rate analyses (Table 4 for Zengcheng and Table 5 for Tumxuk) reveal that the highest growth rates occurred at different stages for each cluster (Figure 14), indicating distinct growth patterns. The average growth rates suggest Cluster 3 in Zengcheng and Cluster 1 in Tumxuk as the fastest-growing, whereas Cluster 2 in both regions exhibited slower growth rates.

Table 4. Growth rate of Zengcheng cotton plant height in each cluster.

Cluster Height (cm/day) Days Range	0–49	49–76	76–82	82–97	97–103	103–108	Mean
0	0.37	1.56	0.83	1.23	0.69	−0.83	0.64
1	0.41	0.94	1.16	0.70	0.48	−0.57	0.52
2	0.39	1.27	1.17	−3.98	−0.01	0.01	−0.19
3	0.55	1.64	1.71	0.79	0.83	−1.00	0.75

Table 5. Growth rate of Tumxuk cotton plant height in each cluster.

Cluster Height (cm/day) Days Range	0–82	82–92	92–107	107–115	115–124	124–147	147–161	Mean
0	0.64	1.74	0.35	1.30	−2.73	0.27	−0.28	0.18
1	0.78	1.58	0.03	1.90	−0.22	0.12	−0.52	0.53
2	0.85	2.24	−0.37	2.06	−6.15	0.32	0.51	−0.08
3	0.90	2.18	−0.09	2.82	−2.97	0.04	−0.84	0.29

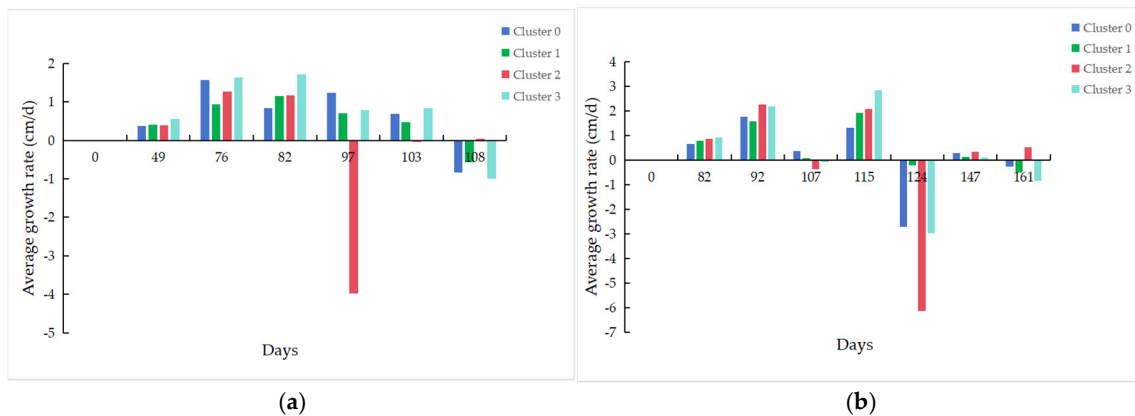


Figure 14. Comparative daily growth rates of each cotton cluster. Panel (a) presents the daily growth rate in centimeters for clusters of cotton varieties in the Zengcheng region, highlighting the variable growth patterns at different developmental stages. Panel (b) shows the analogous daily growth rate for clusters in the Tumxuk region. These representations provide a clear visualization of growth rate disparities among clusters over time.

4. Discussion

This study embarked on a comprehensive exploration of utilizing point cloud data, facilitated through preprocessing techniques, and employing both the Cloth Simulation Filter (CSF) and Progressive TIN Densification (PTD) algorithms for segmenting point clouds to generate Digital Surface Models (DSMs) and Digital Elevation Models (DEMs). The subsequent derivation of the Canopy Height Model (CHM) and matching it with the ground truth coordinates enabled precise cotton plant height information extraction.

4.1. Cotton Plant Height Information Extraction

The comparative analysis reveals that the PTD algorithm consistently outperformed the CSF algorithm in both Zengcheng and Tumxuk. This superior performance is attributed to the PTD algorithm's efficacy in distinguishing between ground and non-ground points, effectively capturing the terrain and plant surface features more accurately. The precision in separating the ground points is crucial for high-density crop height extraction, as demonstrated by the PTD algorithm's higher accuracy; this further verifies the effectiveness of the PTD algorithm [34,40].

The decline in accuracy (R^2 from 0.74 to 0.69) of the PTD algorithm across different growth stages—flowering, boll-forming, and boll-opening—highlights the impact of an

increasing plant density and instances of plant lodging on the quantity of the canopy-intercepted point clouds. This densification and structural changes in the cotton plants lead to a scarcity of ground points, adversely affecting the accuracy of the DEM model and consequently the precision of plant height extraction.

4.2. Cotton Plant Height Growth Dynamics

The analysis using the PTD algorithm elucidates the growth behavior of different cotton varieties in Zengcheng and Tumxuk. Cluster analysis helped discern the growth patterns, with certain clusters showing a stronger growth performance. The findings underscore the variability in the growth dynamics across different cotton varieties and regions, providing valuable insights for agricultural management and varietal selection [41].

The comparison of the plant height means and growth rates between Zengcheng and Tumxuk indicated varietal responses to environmental conditions. Notably, adverse weather conditions, such as heavy rainfall in Zengcheng and sandstorms in Tumxuk, significantly impacted plant growth and survival. These observations point to the critical influence of environmental factors and varietal resilience on cotton growth dynamics [42,43].

The study encountered several challenges, including negative growth rates and reduced survival rates among the 306 cotton varieties tested. The findings suggest that environmental adversities, poor lodging resistance, and soil incompatibility are the primary factors affecting plant growth and survival. The observed varietal decline from emergence to the boll-opening stage underlines the necessity of selecting environmentally adaptable and resilient cotton varieties for cultivation in diverse agricultural landscapes.

5. Conclusions

In this study, the application of UAV remote sensing technology to cotton height information extraction across growth cycles demonstrates significant potential for enhancing precision agriculture practices. In constructing Canopy Height Models (CHMs) using Kriging, the Progressive TIN Densification (PTD) algorithm demonstrated greater accuracy than the Cloth Simulation Filter (CSF) method in both the Zengcheng and Tumxuk trial areas. This advancement offers a rapid and efficient means for large-scale monitoring of cotton growth, essential for optimizing agricultural production and management.

The PTD algorithm's superior accuracy (R^2 0.82) in height extraction underscores its utility in precision agriculture, facilitating the rapid and accurate monitoring of cotton growth.

Cluster analysis of the growth dynamics provided valuable insights into varietal performance and regional adaptability, critical for selecting superior cotton varieties and enhancing crop management strategies.

Future research should focus on refining the extraction algorithms and expanding varietal testing to identify the cotton varieties best suited to different environmental conditions. This approach holds promise to significantly improve cotton production efficiency and sustainability, contributing to the advancement of precision agriculture in China and potentially globally.

Author Contributions: W.Y.: writing, conceptualization, methodology, software. J.W.: writing, conceptualization, methodology, software. W.X.: investigation, software. H.L.: conceptualization, methodology. X.L.: methodology, software. Y.L. (Yubin Lan): conceptualization, funding acquisition, supervision. Y.L. (Yuanhong Li): methodology, funding acquisition, supervision. L.Z.: conceptualization, revision, funding acquisition. All authors have read and agreed to the published version of the manuscript.

Funding: This work was supported by the Laboratory of Lingnan Modern Agriculture Project, China (NT2021009); the China Agriculture Research System (CARS-15-22); the Key Area Research and Development Program of Guangdong Province, China (2019B020214003); the Guangdong Technical System of Peanut and Soybean Industry, China (2019KJ136-05); and the 111 Project (D18019).

Data Availability Statement: Data are available on request from the authors.

Conflicts of Interest: The authors declare no conflicts of interest.

References

1. Yang, W.; Xu, W.; Yan, K.; Cui, Z.; Chen, P.; Zhang, L.; Lan, Y. GEE-Based monitoring method of key management nodes in cotton production. *Int. J. Digit. Earth* **2023**, *16*, 1907–1922. [[CrossRef](#)]
2. Chen, P.; Xu, W.; Zhan, Y.; Wang, G.; Yang, W.; Lan, Y. Determining application volume of unmanned aerial spraying systems for cotton defoliation using remote sensing images. *Comput. Electron. Agric.* **2022**, *196*, 106912. [[CrossRef](#)]
3. Pei, S.; Zeng, H.; Dai, Y.L.; Bai, W.; Fan, J. Nitrogen nutrition diagnosis for cotton under mulched drip irrigation using unmanned aerial vehicle multispectral images. *J. Integr. Agric.* **2023**, *22*, 2536–2552. [[CrossRef](#)]
4. Lin, Y.; Zhu, Z.; Guo, W.; Sun, Y.; Yang, X.; Kovalsky, V. Continuous Monitoring of Cotton Stem Water Potential using Sentinel-2 Imagery. *Remote Sens.* **2020**, *12*, 1176. [[CrossRef](#)]
5. Xiao, Q.; Xin, F.; Lou, Z.; Zhou, T.; Wang, G.; Han, X.; Lan, Y.; Fu, W. Effect of Aviation Spray Adjuvants on Defoliant Droplet Deposition and Cotton Defoliation Efficacy Sprayed by Unmanned Aerial Vehicles. *Agronomy* **2019**, *9*, 217. [[CrossRef](#)]
6. Yang, X.; Wang, Y.; Yin, T.; Wang, C.; Lauret, N.; Regaieg, O.; Xi, X.; Gastellu-Etchegorry, J.P. Comprehensive LiDAR simulation with efficient physically-based DART-Lux model (I): Theory, novelty, and consistency validation. *Remote Sens. Environ.* **2022**, *272*, 112952. [[CrossRef](#)]
7. Lin, Y.; Habib, A. Quality control and crop characterization framework for multi-temporal UAV LiDAR data over mechanized agricultural fields. *Remote Sens. Environ.* **2021**, *256*, 112299. [[CrossRef](#)]
8. Zhao, X.; Guo, Q.; Su, Y.; Xue, B. Improved progressive TIN densification filtering algorithm for airborne LiDAR data in forested areas. *ISPRS-J. Photogramm. Remote Sens.* **2016**, *117*, 79–91. [[CrossRef](#)]
9. Li, W.; Niu, Z.; Wang, C.; Huang, W.; Chen, H.; Gao, S.; Li, D.; Muhammad, S. Combined Use of Airborne LiDAR and Satellite GF-1 Data to Estimate Leaf Area Index, Height, and Aboveground Biomass of Maize During Peak Growing Season. *IEEE J. Sel. Top. Appl. Earth Observ. Remote Sens.* **2015**, *8*, 4489–4501. [[CrossRef](#)]
10. Yuan, W.; Li, J.; Bhatta, M.; Shi, Y.; Baenziger, P.S.; Ge, Y. Wheat Height Estimation Using LiDAR in Comparison to Ultrasonic Sensor and UAS. *Sensors* **2018**, *18*, 3731. [[CrossRef](#)]
11. Madec, S.; Baret, F.; de Solan, B.; Thomas, S.; Dutartre, D.; Jezequel, S.; Hemmerlé, M.; Colombeau, G.; Comar, A. High-Throughput Phenotyping of Plant Height: Comparing Unmanned Aerial Vehicles and Ground LiDAR Estimates. *Front. Plant Sci.* **2017**, *8*, 2002. [[CrossRef](#)] [[PubMed](#)]
12. Hmida, S.B.; Kallel, A.; Gastellu, E.J.P.; Roujean, J.L. Crop Biophysical Properties Estimation Based on LiDAR Full-Waveform Inversion Using the DART RTM. *IEEE J. Sel. Top. Appl. Earth Observ. Remote Sens.* **2017**, *10*, 4853–4868. [[CrossRef](#)]
13. Estornell, J.; Ruiz, L.A.; Velazquez-Martí, B.; Lopez-Cortes, I.; Salazar, D.; Fernandez-Sarria, A. Estimation of pruning biomass of olive trees using airborne discrete-return LiDAR data. *Biomass Bioenergy* **2015**, *81*, 315–321. [[CrossRef](#)]
14. Buunk, T.; Vélez, S.; Ariza-Sentís, M.; Valente, J. Comparing Nadir and Oblique Thermal Imagery in UAV-Based 3D Crop Water Stress Index Applications for Precision Viticulture with LiDAR Validation. *Sensors* **2023**, *23*, 8625. [[CrossRef](#)] [[PubMed](#)]
15. Caruso, G.; Zarco-Tejada, P.J.; González-Dugo, V.; Moriondo, M.; Tozzini, L.; Palai, G.; Rallo, G.; Hornero, A.; Primicerio, J.; Gucci, R. High-resolution imagery acquired from an unmanned platform to estimate biophysical and geometrical parameters of olive trees under different irrigation regimes. *PLoS ONE* **2019**, *14*, e0210804. [[CrossRef](#)] [[PubMed](#)]
16. Xu, W.; Yang, W.; Wu, J.; Chen, P.; Lan, Y.; Zhang, L. Canopy Laser Interception Compensation Mechanism—UAV LiDAR Precise Monitoring Method for Cotton Height. *Agronomy* **2023**, *13*, 2584. [[CrossRef](#)]
17. Han, X.; Thomasson, J.A.; Bagnall, G.C.; Pugh, N.A.; Horne, D.W.; Rooney, W.L.; Jung, J.; Chang, A.; Malambo, L.; Popescu, S.C.; et al. Measurement and Calibration of Plant-Height from Fixed-Wing UAV Images. *Sensors* **2018**, *18*, 4092. [[CrossRef](#)] [[PubMed](#)]
18. Hassan, M.A.; Yang, M.; Fu, L.; Rasheed, A.; Zheng, B.; Xia, X.; Xiao, Y.; He, Z. Accuracy assessment of plant height using an unmanned aerial vehicle for quantitative genomic analysis in bread wheat. *Plant Methods* **2019**, *15*, 37. [[CrossRef](#)] [[PubMed](#)]
19. Lou, Z.; Xin, F.; Han, X.; Lan, Y.; Duan, T.; Fu, W. Effect of Unmanned Aerial Vehicle Flight Height on Droplet Distribution, Drift and Control of Cotton Aphids and Spider Mites. *Agronomy* **2018**, *8*, 187. [[CrossRef](#)]
20. Feng, G.; Yao, Y.; Luo, H.; Zhang, Y.; Du, M.; Zhang, W.; Xia, D.; Dong, H. Canopy light distribution and its correlation with photosynthetic production in super-high yielding cotton fields of Xinjiang, Northwest China. *Ying Yong Sheng Tai Xue Bao J. Appl. Ecol.* **2012**, *23*, 1286–1294.
21. Sultana, F.; Dev, W.; Xin, M.; Han, Y.; Feng, L.; Lei, Y.; Yang, B.; Wang, G.; Li, X.; Wang, Z.; et al. Competition for Light Interception in Different Plant Canopy Characteristics of Diverse Cotton Cultivars. *Genes* **2023**, *14*, 364. [[CrossRef](#)] [[PubMed](#)]
22. Wang, Q.; Chen, H.; Han, Y.; Xing, F.; Wang, Z.; Feng, L.; Wang, G.; Yang, B.; Lei, Y.; Xiong, S.; et al. Effect of Spatial-Temporal Light Competition on Cotton Yield and Yield Distribution. *Agronomy* **2021**, *11*, 2346. [[CrossRef](#)]
23. Ball, R.; Oosterhuis, D.; Mauromoustakos, A. Growth Dynamics of the Cotton Plant during Water-Deficit Stress. *Agron. J.* **1994**, *86*, 788–795. [[CrossRef](#)]
24. Pettigrew, W. Physiological Consequences of Moisture Deficit Stress in Cotton. *Crop Sci.* **2004**, *44*, 1265–1272. [[CrossRef](#)]
25. Qiu, Q.; Sun, N.; Bai, H.; Wang, N.; Fan, Z.; Wang, Y.; Meng, Z.; Li, B.; Cong, Y. Field-Based High-Throughput Phenotyping for Maize Plant Using 3D LiDAR Point Cloud Generated With a “Phenomobile”. *Front. Plant Sci.* **2019**, *10*, 554. [[CrossRef](#)] [[PubMed](#)]
26. Chen, C.; Guo, J.; Wu, H.; Li, Y.; Shi, B. Performance Comparison of Filtering Algorithms for High-Density Airborne LiDAR Point Clouds over Complex LandScapes. *Remote Sens.* **2021**, *13*, 2663. [[CrossRef](#)]
27. Sun, S.; Li, C.; Paterson, A.; Jiang, Y.; Xu, R.; Robertson, J.S.; Snider, J.; Chee, P. In-field High Throughput Phenotyping and Cotton Plant Growth Analysis Using LiDAR. *Front. Plant Sci.* **2018**, *9*, 16. [[CrossRef](#)] [[PubMed](#)]

28. Sun, S.; Li, C.; Paterson, A. In-Field High-Throughput Phenotyping of Cotton Plant Height Using LiDAR. *Remote. Sens.* **2017**, *9*, 377. [[CrossRef](#)]
29. Li, W.; Niu, Z.; Huang, N.; Wang, C.; Gao, S.; Wu, C. Airborne LiDAR technique for estimating biomass components of maize: A case study in Zhangye City, Northwest China. *Ecol. Indic.* **2015**, *57*, 486–496. [[CrossRef](#)]
30. Su, W.; Zhang, M.; Liu, J.; Sun, Z. Automated extraction of corn leaf points from unorganized terrestrial LiDAR point clouds. *Int. J. Agric. Biol. Eng.* **2018**, *11*, 166–170. [[CrossRef](#)]
31. Hui, Z.; Li, D.; Jin, S.; Ziggah, Y.Y.; Wang, L.; Hu, Y. Automatic DTM extraction from airborne LiDAR based on expectation-maximization. *Opt. Laser Technol.* **2019**, *112*, 43–55. [[CrossRef](#)]
32. Zhang, W.; Qi, J.; Wan, P.; Wang, H.; Xie, D.; Wang, X.; Yan, G. An Easy-to-Use Airborne LiDAR Data Filtering Method Based on Cloth Simulation. *Remote Sens.* **2016**, *8*, 501. [[CrossRef](#)]
33. Serifoglu Yilmaz, C.; Yilmaz, V.; Gungor, O. Ground Filtering of a UAV-based Point cloud with the Cloth Simulation Filtering Algorithm. In Proceedings of the International Conference on Advances and Innovations in Engineering (ICAIE), Elazig, Turkey, 10–12 May 2017.
34. Shi, X.; Ma, H.; Chen, Y.; Zhang, L.; Zhou, W. A parameter-free progressive TIN densification filtering algorithm for lidar point clouds. *Int. J. Remote Sens.* **2018**, *39*, 6969–6982. [[CrossRef](#)]
35. Stroner, M.; Urban, R.; Kremen, T.; Braun, J. UAV DTM acquisition in a forested area—Comparison of low-cost photogrammetry (DJI Zenmuse P1) and LiDAR solutions (DJI Zenmuse L1). *Eur. J. Remote Sens.* **2023**, *56*, 2179942. [[CrossRef](#)]
36. Diara, F.; Roggero, M. Quality Assessment of DJI Zenmuse L1 and P1 LiDAR and Photogrammetric Systems: Metric and Statistics Analysis with the Integration of Trimble SX10 Data. *Geomatics* **2022**, *2*, 254–281. [[CrossRef](#)]
37. Teppati Losè, L.; Matrone, F.; Chiabrandò, F.; Giulio Tonolo, F.; Lingua, A.; Maschio, P. New developments in lidar uas surveys. performance analyses and validation of the dji zenmuse L1. *Int. Arch. Photogramm. Remote Sens. Spat. Inf. Sci.* **2022**, *XLIII-B1-2022*, 415–422. [[CrossRef](#)]
38. Cai, S.; Liang, X.; Yu, S. A Progressive Plane Detection Filtering Method for Airborne LiDAR Data in Forested Landscapes. *Forests* **2023**, *14*, 498. [[CrossRef](#)]
39. Thorndike, R.L. Who belongs in the family? *Psychometrika* **1953**, *18*, 267–276. [[CrossRef](#)]
40. Sabirova, A.; Rassabin, M.; Fedorenko, R.; Afanasyev, I. Ground Profile Recovery from Aerial 3D LiDAR-Based Maps. In Proceedings of the 2019 24th Conference of Open Innovations Association (FRUCT), Moscow, Russia, 8–12 April 2019; pp. 367–374.
41. Irene, B.; Tom, D.S.; Paul, Q.; Jonas, A.; Aamir, S.; Wouter, S.; Ben, S.; Isabel, R.; Peter, L. Closing the Phenotyping Gap: High Resolution UAV Time Series for Soybean Growth Analysis Provides Objective Data from Field Trials. *Remote Sens.* **2020**, *12*, 1644. [[CrossRef](#)]
42. Sadras, V.; Bange, M.; Milroy, S. Reproductive allocation of cotton in response to plant and environmental factors. *Ann. Bot.* **1997**, *80*, 75–81. [[CrossRef](#)]
43. Baig, K.S.; Ali, Z.; Warraich, I.A.; Khan, S.U.; Kausar, R.; Kashaf, A.; Gul, N.; Khan, O.U.; Nawaz, R.; Ahmad, H.T. Sustainable cotton cultivation in saline soils: Challenges, innovations, and future prospects. *Biol. Clin. Sci. Res. J.* **2023**, *2023*, 584. [[CrossRef](#)]

Disclaimer/Publisher’s Note: The statements, opinions and data contained in all publications are solely those of the individual author(s) and contributor(s) and not of MDPI and/or the editor(s). MDPI and/or the editor(s) disclaim responsibility for any injury to people or property resulting from any ideas, methods, instructions or products referred to in the content.